ACS OMEGA

Open Access

This article is licensed under CC-BY 4.0

http://pubs.acs.org/journal/acsodf

Article

Beta Irradiation Effects on Electrical Characteristics of Graphene-Doped PVA/n-type Si Nanostructures

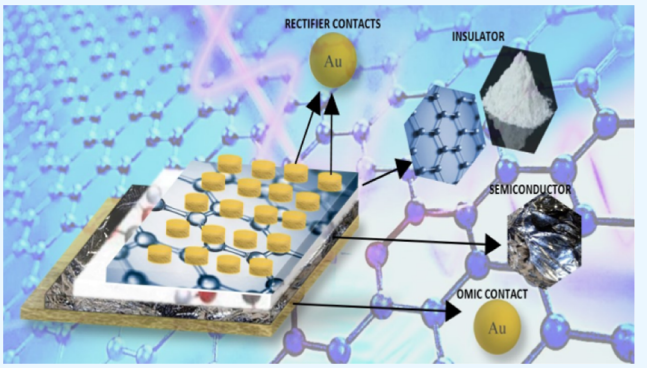
Özlem Abay, Murat Ulusoy, Esra Uyar, Uğur Gökmen, and Sema Bilge Ocak*

Cite This: *ACS Omega* 2024, 9, 23193−23201

Read Online

ACCESS | Metrics & More | Article Recommendations

ABSTRACT: This study investigates the beta irradiation's impact on the electrical features of interfacial nanostructures composed of poly(vinyl alcohol) (PVA) doped with graphene. The integration of graphene, a 2D carbon allotrope renowned for its exceptional electrical conductivity, into PVA nanostructures holds significant promise for advanced electronic applications. Beta irradiation, as a controlled method of introducing radiation, offers a unique avenue to modulate the properties of these nanostructures. Therefore, this study examines the Au/3% graphene(Gr)-doped PVA/n-type Si structure with and without beta (β) radiation. The effect of beta radiation on the electrical properties of the Au/3% graphene(Gr)-doped PVA/n-type Si structure has been researched by utilizing the current−voltage ($I-V$) data. The studied structures were exposed to a ^{90}Sr β-ray source at room temperature to show the effect of beta radiation. The series resistance (R_s), shunt resistance (R_{sh}), ideality factor (n), barrier height (BH) (Φ_{B0}), and saturation current (I_o) were computed using the $I-V$ data after ^{90}Sr β-ray irradiation (0, 6, and 18 kGy) and before using the thermionic emission, Norde, and Cheung methods. The BH, ideality factor, and series resistance were calculated using the $I-V$ data as follows: 0.888 eV, 3.21, and 5.25 kΩ for 0 kGy; 0.782 eV, 5.30, and 3.47 for 6 kGy; 0.782 eV, 5.46, and 2.63 kΩ for 18kGy. The BH, ideality factor, and series resistance were also calculated using the Cheng Methods, and the following results were found respectively: 7.22, 0.74, and 3.97 kΩ (Cheng I), and 3.22 kΩ (Cheng II) for 0 kGy; 5.14, 0.813, and 2.72 kΩ (Cheng I), and 2.14 kΩ (Cheng II) for 6 kGy; 6.78, 0.721, and 1.96 kΩ (Cheng I), 1.64 kΩ (Cheng II) for 18 kGy. The BH and series resistance were defined as 0.905 and 16.12 kΩ for 0 kGy, 0.859 and 5.31 kΩ for 6 kGy, and 0.792 and 2.49 kΩ for 18 kGy, respectively. Interface states density (N_{ss}) as a function of E_c-E_{ss} was also attained by taking into account the voltage dependence of n, Φ_B, and R_s. Experimental results showed that the values of n and N_{ss} increased with an increase in the β-ray radiation dose. On the other hand, the saturation current (I_o), Φ_{B0}, and R_s values decreased with the increase in the β-ray radiation dose. The obtained results indicate a nuanced interplay between β irradiation dose and the nanostructure's overall electrical properties. Insights gained from this study contribute to the understanding of radiation-induced effects on graphene-doped polymer nanostructures, providing valuable information for optimizing their performance in electronic applications.



Downloaded via 176.33.244.6 on January 7, 2025 at 19:38:25 (UTC).
See https://pubs.acs.org/sharingguidelines for options on how to legitimately share published articles.

1. INTRODUCTION

The semiconductor industry has spent the last 40 years trying to form nanoelectronic devices with improved performance. Semiconductor radiation detectors, which are used for various applications and fabricated from costly high-purity inorganic crystals, such as germanium and silicon, ensure higher energy resolution compared to radiation detectors of other types. In recent years, organic semiconductors have facilitated the development of various organic electronic devices in the traditional electronics fields.[1−6] There has been growing interest in exploring novel materials and nanostructures for advanced electronic applications, driven by the continuous quest for improved device performance and functionality. Graphene, a hydrogenated derivative of graphene, has emerged as a promising candidate due to its unique electronic properties and compatibility with various substrates. Allotropes of carbon-based nanomaterials with distinctive electrical characteristics, such as carbon nanotubes (CNT) and graphene foils, have been developed for commercial use.[7] Application to technologies for radiation detection has also been encouraged.[8] The electrical conductivity per unit charge, which is defined by charge carrier mobility, exhibits a considerable effect on the sensitivity of radiation detectors.[7−11] One such intriguing application involves the integration of graphene into poly(vinyl

Received: October 28, 2023
Revised: March 23, 2024
Accepted: May 10, 2024
Published: May 20, 2024



© 2024 The Authors. Published by American Chemical Society

alcohol) (PVA)/n-type silicon (Si) nanostructures, offering a synergistic platform for innovative electronic devices.

Organic synthesis allows for the versatile design of a broad spectrum of organic semiconductors, presenting several advantages due to their noncorrosive nature, flexibility, and cost-effectiveness. These attributes make organic semiconductors particularly appealing for applications for which traditional materials, such as metals, may be less suitable. In large-area electronic devices, such as capacitors and organic electroluminescence (EL) devices, the use of organic semiconductors can contribute to cost reduction and increased flexibility, facilitating their incorporation into diverse environments.[12−15]

Despite these advantages, the proliferation of electronic devices in various settings exposes them to external factors including radiation. Beta irradiation, characterized by the emission of high-energy electrons, poses a notable environmental challenge that electronic components may confront. The intricate interaction between beta radiation and nanostructured materials can lead to complex effects on the electrical characteristics of these materials. Such effects have the potential to influence the overall performance and reliability of electronic devices.

As electronic technologies continue to advance, understanding the impact of radiation on novel materials, especially organic semiconductors, becomes imperative. Investigating the response of organic semiconductors to beta irradiation is crucial for evaluating their suitability in radiation-prone environments and optimizing their performance under such conditions. This exploration not only contributes to the fundamental understanding of the behavior of organic semiconductors under radiation exposure but also guides the development of radiation-resistant electronic components for diverse applications. It is anticipated that organic semiconductors will contribute to the development of low-cost and flexible radiation detectors with large detection zones. Several studies have been carried out to develop a real-time radiation detector using the electroconductive polymer polyaniline (Pani). The real-time radiation detector was successful in detecting the α and β particles.[16,17] However, the sensor sensitivity of the device is still weak. Especially, its sensitivity for detecting β particles must be developed before it can be used for practical purposes. Among the various polymeric materials, poly(vinyl) alcohol (PVA) is a water-soluble, nontoxic, and semi-crystalline polymer. Moreover, the PVA polymer has a wide range of crystallinity, low conductivity, good charge storage capacity, very high dielectric strength, and interesting physical characteristics. In this regard, PVA is one of the most significant polymer materials used as an organic interface material in the construction of electronic devices. High conductivity, low dielectric loss, and high dielectric constant can be achieved by alloying the PVA polymer with suitable metals or graphene.

Metal−polymer/insulator−semiconductor (MPS/MIS) devices have interfacial states (N_{ss}), series resistance (R_s), the series resistance, and the interfacial layer, and the voltage applied to this material is dealt with over the layer of depletion. The electrical characteristics of these structures are therefore different from their ideal behavior under conditions such as lighting or radiation. Namely, the optical and electrical properties of the MPS/MIS structures are significantly dependent on N_{ss}, R_s, and radiation as well as the applied electric field, the doping, and the interfacial layer of the semiconductor devices. However, the surface states between the interfacial layer and semiconductor act as recombination centers, and they are capable of capturing or releasing electrical charges under the radiation or electric field. Such recombination centers also offer a tunnel road for the carriers. Though electron−hole pairs are formed by radiation in the semiconductor, only the holes can diffuse into the interface layer because their mobility is smaller compared to electrons that get out of the interface or recombine with holes. On the contrary, the radiation does not have adequate energy to generate electron−hole pairs, so many energetic particles and photons go right through the device without being absorbed by the semiconductor devices.[18,19] Until now, ionizing radiation's effects on semiconductor devices have already been the subject of several studies.[20−22] However, the literature has a limited number of studies on the consequences of simultaneous voltage and radiation alterations. Furthermore, the effect of radiation on materials varies significantly if different materials are used as interlayers or if the dose and/or type of radiation varies.

MS contacts are crucial and good experimental instruments for researching the interactions and effects of ionizing radiation on interfaces despite the radiation hardness testing and reliability concerns. Different radiation types, such as swift heavy ions (SHI), cosmic rays, and low energy ions (γ rays, protons, alpha particles, neutrons, and electrons), have different effects on electronics via various methods. High-energy ions interact with the target substance and lose most of their energy there. Elastic collisions (atomic energy loss) are observed toward the entry of the ion field first, and then inelastic collisions (electron energy loss) are observed close to the entrance. Each type of energy loss mechanism has a different impact on the interface. Nuclear energy loss results in sporadic faults at interfaces, whereas electronic energy loss forms zones of complex faults in the materials, and it is also known to result in the annealing of faults.[23−25] The motivation behind investigating the beta irradiation on the electrical characteristics of graphene-doped PVA/n-type Si nanostructures for radiation sensors lies in the imperative to enhance the performance and reliability of radiation detection technologies. Beta irradiation, characterized by the emission of high-energy electrons, represents a significant environmental challenge that electronic components, particularly radiation sensors, may encounter. By studying the effects of beta irradiation on the electrical characteristics of graphene-doped PVA/n-type Si nanostructures, researchers aim to gain insights into how these materials respond to radiation exposure. This understanding is crucial for optimizing the design and composition of radiation sensors, ensuring their accuracy, sensitivity, and stability in real-world applications. The research contributes not only to advancements in nanotechnology but also to the development of radiation sensors that play a vital role in various fields including nuclear facilities, medical settings, and environmental monitoring, ultimately enhancing safety and reliability in radiation detection.

The motivation behind the study is to explore and understand how beta irradiation affects the electrical characteristics of a specific type of nanostructure: graphene-doped PVA/n-type Si nanostructures.

To our knowledge, the literature does not have a detailed study on the impact of ^{90}Sr beta (β) rays on the electrical properties of the Au/n-Si structures with Gr-doped PVA interfacial layers. This study aims to obtain high-performance Au/n-type Si structures with a 3% Gr-doped PVA interfacial

https://doi.org/10.1021/acsomega.3c08449
ACS Omega 2024, 9, 23193−23201

layer after and before ^{90}Sr β-ray irradiation. To investigate the effect of the ^{90}Sr β-ray irradiation on these structures' electrical features, we measured the $I-V$ properties before and after exposing them to the ^{90}Sr β-ray irradiation at room temperature. We calculated the values of the series resistance, ideality factor, interface state, saturation current, shunt resistance, and barrier height (BH) using the standard, Cheung, and Norde functions for the cases before and after ^{90}Sr beta (β) irradiation. Then, we compared these values.

2. EXPERIMENTAL DETAILS

Au/3% Gr-doped PVA/n-type Si was grown on the phosphor-doped (4.3×10^{15} cm^{-3}) n-type Si wafer with an orientation of (100), diameter of 2 in., thickness of 350 nm, doping donor atoms (N_C) of 2.8×10^{19} cm^{-3}, and resistivity of 0.5 Ω cm. Details about the chemical cleaning processes of the n-Si wafer, as well as the formation and deposition of the doped-polymer (Gr-PVA) organic thin film, were provided in the previous study.[26] Figure 1 presents the schematic diagram of the

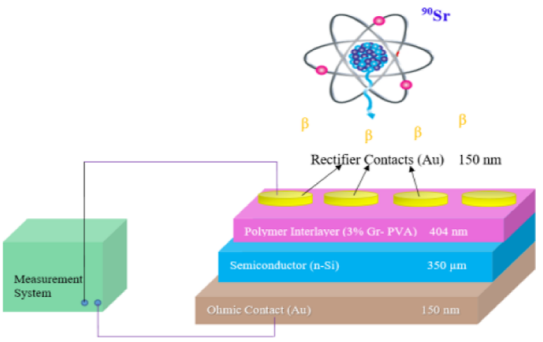


Figure 1. Au/3% Gr-doped PVA/n-type Si structures schematic diagram.

fabricated Au/3% Gr-doped PVA/n-type Si (MPS) structure. Keithley 2400 Source Meter was used to measure the $I-V$ values for revealing the structure's electrical properties at room temperature. Then, the Au/3% Gr-doped PVA/n- type Si (MPS) structure was exposed to high radiation with 6 and 18 kGy using ^{90}Sr β-ray irradiation. Finally, the $I-V$ values of these structures were measured again using the same Keithley 2400 Source Meter.

3. RESULTS AND DISCUSSION

The electrical properties of PVA doped with 3% graphene nanostructure are defined using the thermionic emission (TE) theory.[18] The widely adopted approach for facilitating the passage of high-energy electrons over the BH (Φ_{B0}) in metal–semiconductor (MS) type Schottky diodes (SDs), whether equipped with or without an interlayer at the M/S interface, is the standard TE theory. In accordance with this theory, when the SD (SD) experiences $V \geq 3kT/q$, the relationship between forward-bias voltage and current can be expressed as follows

$$I(V) = I_0\left[\exp\left(\frac{q(V - IR_s)}{nkT}\right) - 1\right] \quad (1)$$

$$I_0 = AA^*T^2\exp\left(\frac{-q\Phi_{B0}}{kT}\right) \quad (2)$$

$$\Phi_{B0} = \frac{kT}{q}\ln\left(\frac{AA^*T^2}{I_0}\right) \quad (3)$$

$$n = \frac{q}{kT}\left[\frac{d(V)}{d(\ln I)}\right] \quad (4)$$

where q, A, A^*,IR_s, k, I_0, and Φ_{B0} denote the electron charge, rectifier contact area (7.85×10^{-3} cm^2), the effective Richardson-constant (=112 A/cm^2 K^2 for n-type Si), the voltage-drop on the R_s (series resistance), Boltzmann constant, reverse saturation current, and the bias BH, respectively. First, the I_0 values were computed for the points at which the ln $I-V$ curves intersect the ln I axis. The linear ranges of I_0 have been defined before and after beta (β) irradiation from approximately 0.05 to 0.35 V. The slopes of the linear parts of the ln $I-V$ curves were calculated by utilizing the reciprocal of the

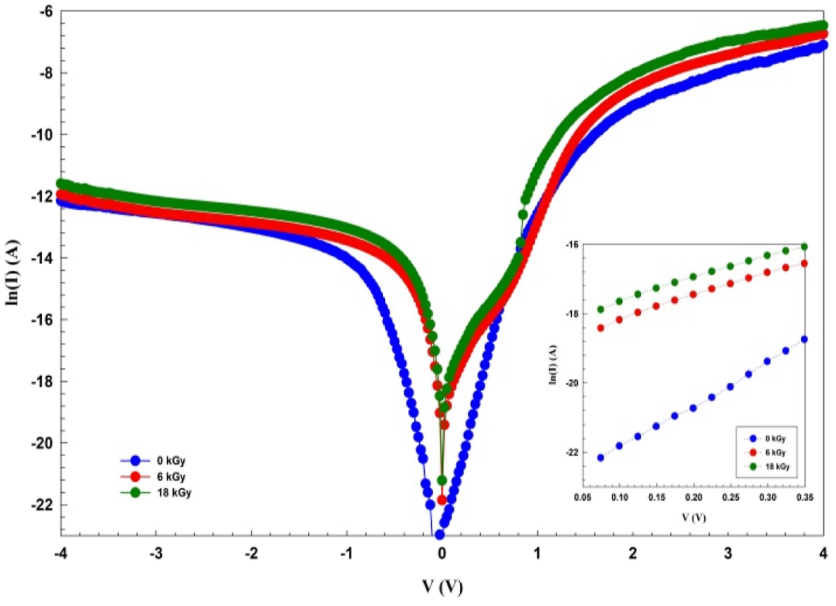


Figure 2. ln I versus V plots of Au/3% Gr-doped PVA/n-type Si diode.

https://doi.org/10.1021/acsomega.3c08449
ACS Omega 2024, 9, 23193−23201

thermal energy (kT/q), and the electrical parameter n was found to deviate significantly from the TE theory. The semilog $I-V$ curves of Au/%3 Gr-doped PVA/n-Si structures before and after beta (β) irradiation (0, 6, 18 kGy) are illustrated in Figure 2 over a large voltage range (±4 V). As shown in the figure, all the ln $I-V$ curves indicate good rectification behavior. While the curves behave linearly well at lower positive voltages, there are bends at higher positive voltages. These bends are caused by the R_s and the organic (Gr:PVA) interface layer.

It is generally assumed that radiation has two types of effects on materials: permanent effects and temporary effects.[18] The temporary effect causes electron−hole pair recombination or radiation-induced generation. On the other hand, the permanent effect, which leads to a change in the crystal lattice structure, is mostly due to radiation bombardment. Besides, irradiated semiconductor devices might have eight effects, where one or a combination of them might have an effect.[27] Eventually, radiation-induced defects, surface traps, recrystallization, dangling bonds, etc. greatly affect the performance of irradiated devices. The measured values must be analyzed in detail for a precise and comprehensive understanding of these effects. Therefore, the effect of radiation on n-Si type SDs doped with 3% Gr-doped PVA was investigated using the $I-V$ characteristics. Figure 2 presents the Au/%3 Gr-doped PVA/n-Si structure's $I-V$ characteristics before irradiation and after different β-irradiation doses (0, 6, and 18 kGy). The linear components of forward bias in this figure also indicate the ln $(I) - V$ properties, which are used in the calculations. The currents are graphed on a logarithmic plot to estimate forward and reverse currents together. The structures in Figure 2 display leakage and current normal rectification behavior with a low turn-on voltage.

The simplest form of Ohm's Law was used to derive R_s and R_{sh} values from the $I-V$ data and plot in Figure 3. Table 1 shows the values of n, I_0, Φ_{B0}, R_{sh}, R_s, and Rectifier rate (RR = $I_{forward}/I_{reverse}$ at ±4 V) of the %3 Gr-doped PVA interfacial layer structures for the cases before and after (β) ray irradiation. The table indicates that n values are greater than unity due to N_{ss}, BH image power reduction, voltage-dependent Φ_{B0}, interfacial layer, and spatial barrier inhomogeneity in the M/S interface. The electron−hole pair generation under the impact of radiation leads to the increase in I_o with β radiation.

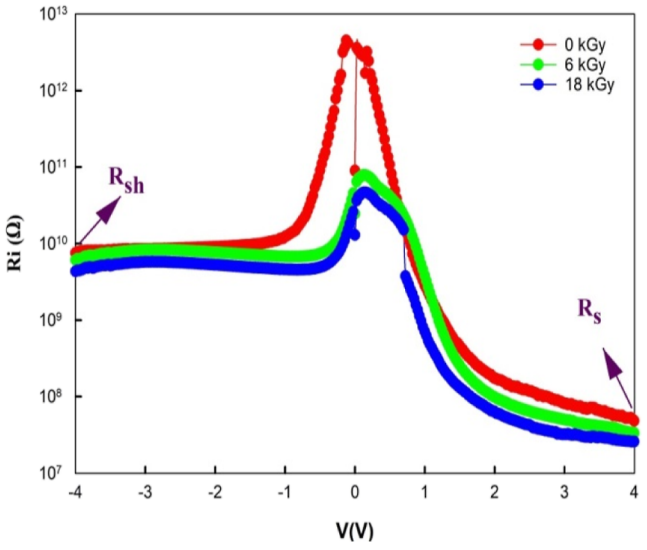


Figure 3. R_i versus V plots of the Au/3% Gr-doped PVA/n-type Si diode.

Since the field in the reverse bias zone is far stronger than that in the forward bias zone, it can prevent electron−hole (e−h) pairs' recombination, which happens during radiation. Even though the R_{sh} value increases with the decrease in β-irradiation, R_s becomes almost constant. On the other hand, a reduction in layer width and a consequent rise in radiation may be the cause of the drop in BH with rising radiation.[28] All the results in Table 1 suggest that β-irradiation is more useful for operating various types of electronic equipment.

The BH and ideality factor are depicted in Figure 4 as a function of β-irradiation. The n values that were determined before and following various dosages of β-irradiation are substantially greater than one. This is because, in addition to TE theory, there are other potential carrier processes (surface state-induced tunneling, diffusion theory, BH, Gaussian distribution, dislocations, and generation-recombination theory).[29]

As illustrated in Figure 5, the relationship between Φ_{B0} and n is defined with the equation of Φ_{B0} (n) = $(-0.0523n + 1.0561)$, and the value of Φ_{B0} for the ideal situation $(n = 1)$ is predicted as 1.004 eV. The existence of graphene is related to the following characteristics: PVA interlayer, thickness, depletion layer width (W_d), donor atom doping concentration (N_d), N_{ss}, and barrier inhomogeneity.[7,8,30−33]

Electron−hole (e−h) pair generation, electron and hole recombination, hole transit, hole trapping, and hole generation on the surfaces of n-type Si semiconductors constitute some of the significant effects of irradiation exposure. The proportion of ray energy that is transformed into electron−hole pairs relies on the characteristics of Gr-doped-PVA because the length of the depletion area is a crucial factor in the generation of electron−hole pairs. In addition, the technique for producing e−h pairs demonstrates how effectively e-h pairs are produced in graphene-doped PVA-based diodes. It is crucial to understand that the fundamental idea behind semiconductor radiation detectors is the generation of e-h pairs in the depletion area.[34−38]

We used Norde and Cheung functions in addition to the TE theory to account for the impact of R_s and Φ_{B0}. The following relationships may be used to compute the three fundamental diode parameters, such as Φ_{B0}, R_s, and n, in a second way at sufficiently high forward bias voltages using the Cheung functions.

First, the Norde function $(F(V))$ is a different way to determine the values of R_s and Φ_{B0}, and this function is stated as follows[32,39]

$$F(V) = \frac{V}{\gamma} - \frac{kT}{q}\left[\ln\left(\frac{I(V)}{A^*AT^2}\right)\right] \quad (5)$$

where γ must be a positive integer greater than n, which has no dimensions. Equation 5 is used to generate the $F(V)$ versus V plots before and after the β-irradiation, and they are displayed in Figure 6. The lowest point of $F_o(V)$ is shown by the concave section in Figure 6, and the voltage associated with it is V_o. Finally, by utilizing the established $F_o(V)$ and V_o values and the related equation below, it is feasible to infer Φ_{B0} and R_S values.

https://doi.org/10.1021/acsomega.3c08449
ACS Omega 2024, 9, 23193−23201

Table 1. Au/3% Gr-Doped PVA/n-type Si Structure's Electrical Parameters Before and After Beta (β) Irradiation Doses

β-irradiation doses (kGy)	n	I_0 (A)	Φ_{B0} (eV)	R_s (kΩ) (+4 V)	R_{sh} (MΩ) (−4 V)	RR
0	3.21	9.86×10^{-11}	0.888	4.85	0.755	155.47
6	5.30	5.91×10^{-9}	0.782	3.36	0.613	182.45
18	5.46	1.03×10^{-8}	0.768	2.59	0.433	167.41

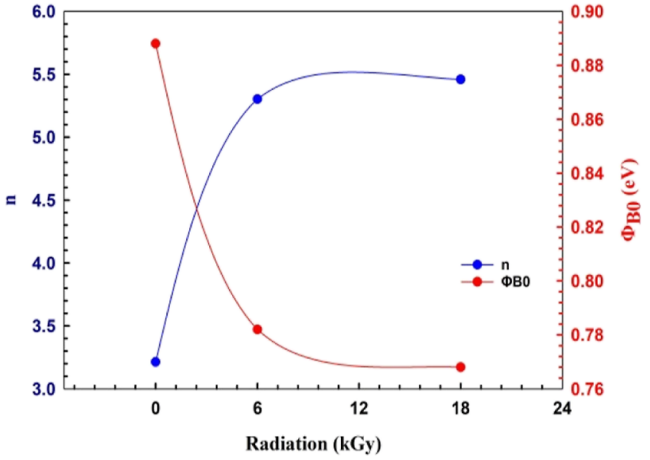


Figure 4. BH and ideality factor depend on β-irradiation.

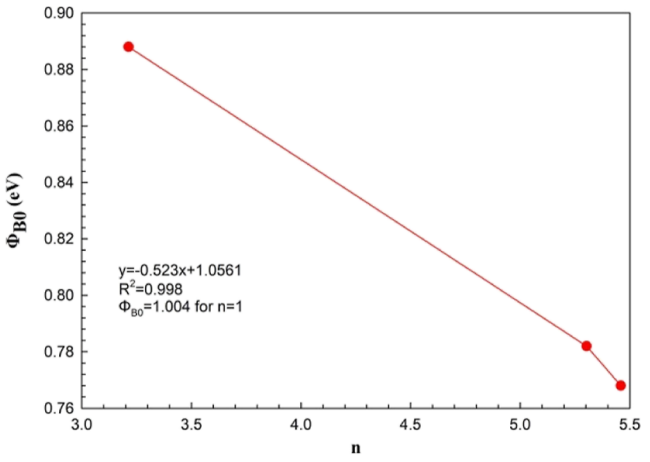


Figure 5. Φ_{B0} vs n plot of the Au/3% Gr-doped PVA/n-type Si diode.

$$\Phi_{B0} = F(V_m) + \frac{V_m}{\gamma} - \frac{kT}{q} \tag{6a}$$

$$R_s = \left(\frac{kT}{q}\right)\left(\frac{\gamma - n}{I_m}\right) \tag{6b}$$

The values of R_s and Φ_{B0} may be calculated via the $F(V)$ vs V plots using the I_m and V_m values that correspond to the lowest value of this plot as illustrated in Figure 6.

Second, according to the Cheung functions, the following relationships may be used to compute the fundamental three SD parameters, namely, R_s, n, and Φ_{B0}, at sufficiently high forward bias voltages.

$$\frac{dV}{d\ln(I)} = \frac{nkT}{q} + IR_s \tag{7a}$$

$$H(I) = V - \frac{nkT}{q}\left[\ln\left(\frac{I}{AA^*T^2}\right)\right] = n\Phi_{B0} + IR_s \tag{7b}$$

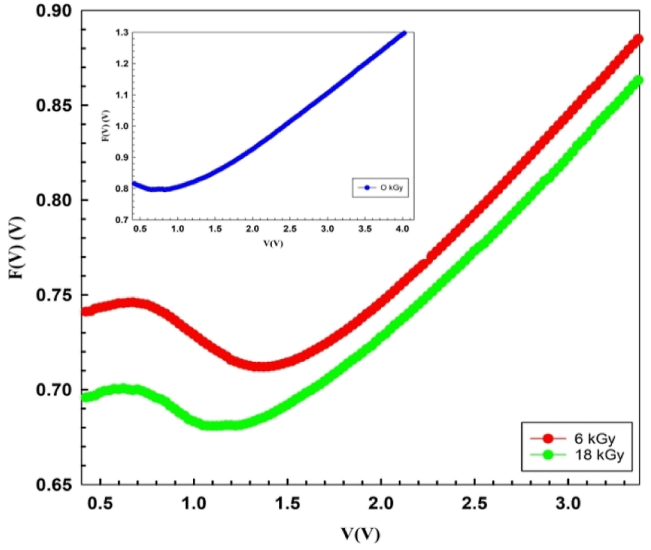


Figure 6. $F(V)$ vs V plots of the Au/3% Gr-doped PVA/n-type Si diode.

Figure 7a−c shows the $dV/d\ln(I)$ and $H(I)$ vs I plots for a diode before and after the β-irradiation using eqs 7a and 7b.

The intersection and slopes of the $dV/d\ln(I)$ vs I plots were calculated using eq 7a to obtain the n and R_s values. Next, $H(I)$ versus I plots were drawn using the n values in eq 7b, and the slope and intersection point of these plots were utilized to calculate the values of R_s and Φ_{B0}. To compare the results from TE, Norde, and Cheung's techniques, the fundamental electrical parameters (n, R_s, and Φ_{B0}) of the diode were reported in Table 2. Due to the different methodologies, these methods are used to derive the voltage-dependent parameters; as indicated in Table 2, there are variations in the results.

Calculating radiation-induced surface states in the band gap requires obtaining the voltage-dependent ideality factor ($n(V)$) and the effective BH (Φ_e). When the R_s impact is ignored, the $n(V)$ and (Φ_e) may be derived using eqs 8a and 8b.[39,40] Thus, by accounting for $n(V)$ and (Φ_e), the N_{ss} formula may be stated as in eq 8d.[41] In these calculations, the $(V - IR_s)$ expression should be used rather than the (V) expression if the R_s effect is taken into account. The terms ε_s and ε_i in these equations stand for the permittivity of the interlayer and semiconductor, respectively. For this diode, the polymer interlayer (graphene−PVA) thickness was found as 404 nm.[42] On the contrary, it is known that eq 8c gives the energy formula from the midgap (E_{ss}) toward the upper edge of the conduction band (E_c).

With the creation of a diode structure, increasing numbers of N_{ss} may form between an interlayer and a semiconductor positioned near the semiconductor's bandgap. These generally result from flaws such as oxygen vacancies, dangling limits that rely on the chemical makeup of the interfacial layer, and other irregularities in the periodic lattice.[21,41,43,44] The use of forward-bias $I-V$ (current−voltage) characteristics, along with consideration for the voltage-dependence of the ideality

https://doi.org/10.1021/acsomega.3c08449
ACS Omega 2024, 9, 23193−23201

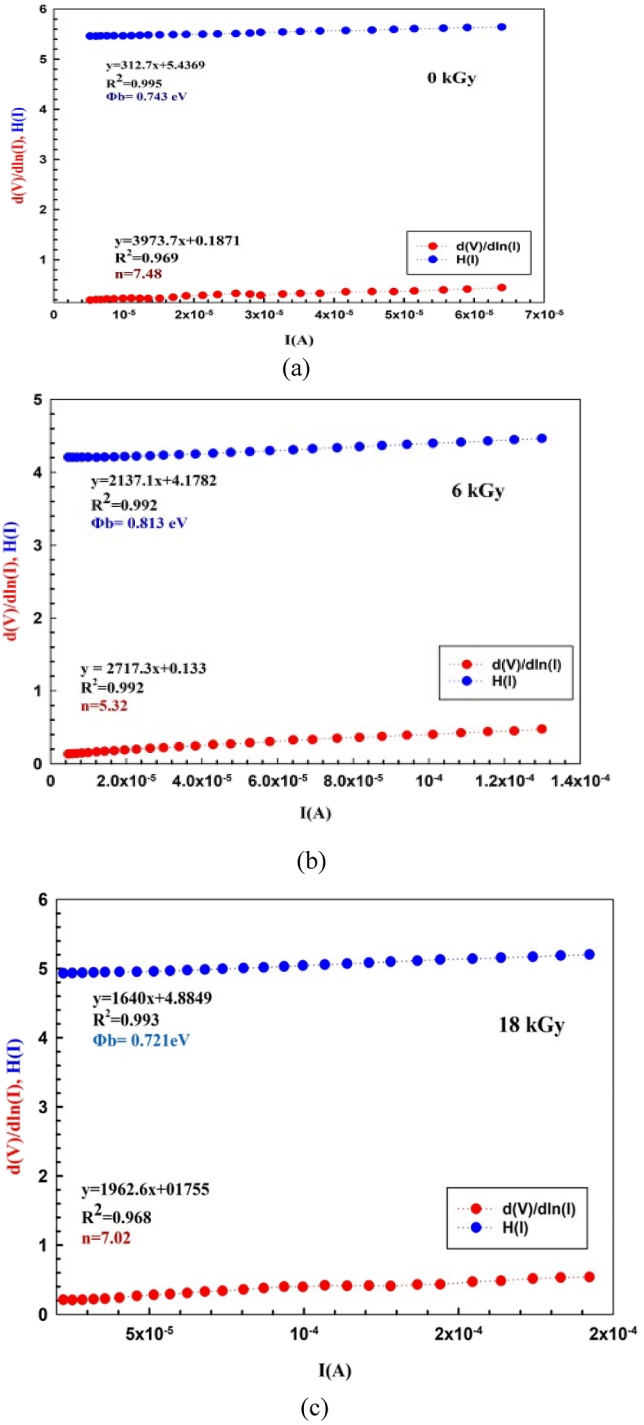


Figure 7. $dV/d\ln(I)$ and $H(I)$ versus I plots the of Au/3% Gr-doped PVA/n-type Si diode (a) for 0 kGy (b) 6 kGy (c) for 18 kGy.

factor (n) and built-in potential Φ_{B0} using a voltage-dependent Φ_e (effective BH) and the equation for n established by Card and Rhoderick, enables the determination of the energy-dependent profile of interface states (N_{ss})

$$n = \frac{q}{kT}\left(\frac{dV}{d(\ln I)}\right) = 1 + \frac{\delta_i}{\varepsilon_i}\left[\frac{\varepsilon_s}{W_D} + qN_{ss}\right] \quad (8a)$$

$$\Phi_e = \Phi_{B0} + \beta(v - IR_s) = \Phi_{B0} + \left(1 - \frac{1}{n(V)}\right)(V - IR_s) \quad (8b)$$

$$E_c - E_{ss} = q(\Phi_e - V) \quad (8c)$$

$$N_{ss}(V) = \frac{1}{q}\left[\frac{\varepsilon_i}{\delta}(n(V) - 1) - \frac{\varepsilon_s}{W_D}\right] \quad (8d)$$

where W_D is the width of the depletion layer, and ε_s (=11.80 for Si) and ε_i (=593) are the electrical permittivity of the semiconductor and interlayer, respectively. δ is the interlayer thickness, which is computed from the interfacial layer capacitance ($C_i = \varepsilon\varepsilon_o A/\delta_i$) as 404 nm. On the other hand, for n-type Si semiconductors, $E_c - E_{ss} = q(\Phi_e - V)$ may be used to describe the energy difference between the level N_{ss} (E_{ss}) and the edge of the conduction band (E_c).[44]

Figure 8 shows the energy-dependent N_{ss} profiles before and following various beta radiation dosages. This figure shows that

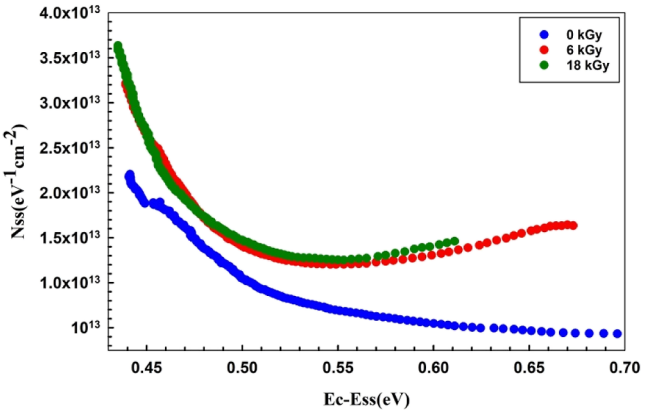


Figure 8. N_{ss} versus ($E_c - E_{ss}$) plots of the Au/3% Gr-doped PVA/n-type Si diode both before and after β-irradiation.

surface states' density declines practically exponentially from the E_{ss} toward the bottom edge of the E_c both before and after irradiation. Additionally, with the increase in the radiation doses, the N_{ss} levels drop, as expected. The variation in N_{ss} behavior can be elucidated by the recombination of electron−hole (e−h) pairs influenced by radiation or the reorganization or restructuring of surface states within the band gap in the presence of an electric field. On the other hand, it can be shown that the N_{ss} values are rather modest when the R_s

Table 2. Au/3% Gr-Doped PVA/n-type Si Diode's Electrical Parameters Using the TE, Cheung, and Norde Functions

irradiation doses (kGy)	$I-V$			Cheung-I		Cheung-II		Norde	
	n	Φ_{B0} (eV)	R_s (kΩ)	n	R_s (kΩ)	Φ_{B0} (eV)	R_s (kΩ)	Φ_{B0} (eV)	R_s (kΩ)
0	3.21	0.888	5.25	7.22	3.97	0.74	3.22	0.905	16.12
6	5.30	0.782	3.47	5.14	2.72	0.813	2.14	0.859	5.31
18	5.46	0.768	2.63	6.78	1.96	0.721	1.64	0.792	2.49

https://doi.org/10.1021/acsomega.3c08449
ACS Omega 2024, 9, 23193−23201

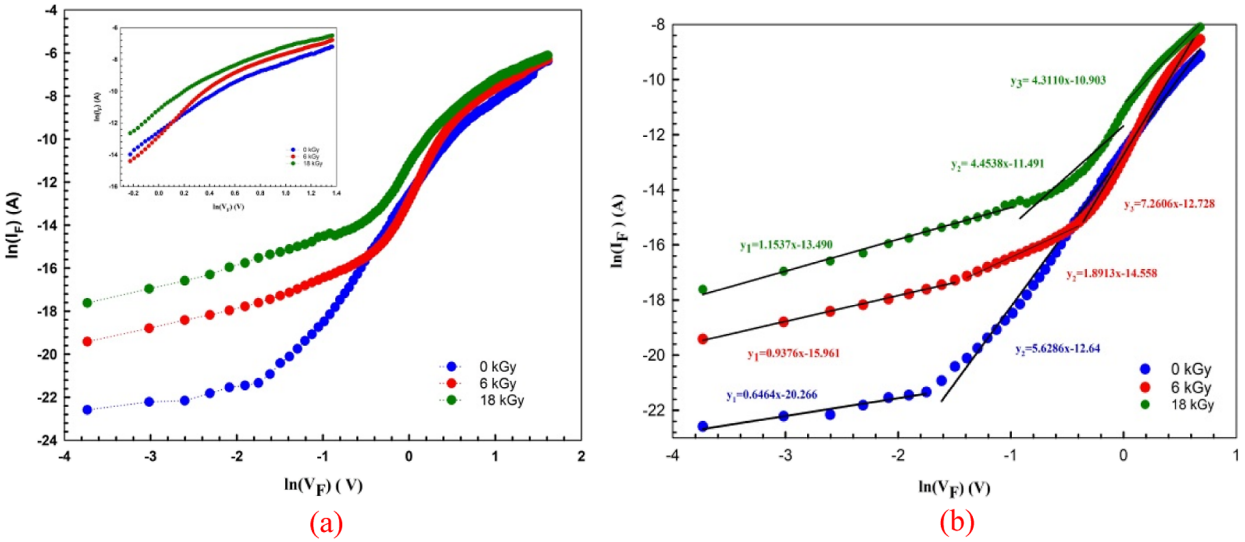


Figure 9. (a) $\ln(I_F) - V_F$ and (b) $\ln(I_F) - V_F$ linear regions of the plot for the Au/3% Gr-doped PVA/n-type Si diode before and after β-irradiation.

impact is taken into consideration. This outcome simply illustrates the significance of R_s in the computations.[45]

Additionally, the impact of the β-irradiation on the free carrier currents and current conduction mechanisms (CCMs) of the diode has been investigated at forward and reverse biases. Figure 9a,b shows the diode's $\ln(I_F) - V_F$ plots, which include several areas corresponding to various CCMs. Generally, shallow and deep traps at the metal−semiconductor contact cause an increase in the charge transfer. As can be seen in Figure 9a,b, the Au/3% Gr-doped- PVA/n-type Si diode's $(\ln(I_F) - V_F)$ plot has three separate linear regions with various slopes after irradiation, as opposed to these diodes' $(\ln(I_F) - V_F)$ plots, which have two distinct linear regions with different slopes before β irradiation. In the first region, these slopes are 0.6464 for 0 kGy, 0.9376 for 6 kGy, and 1.1537 for 18 kGy. In the second region, they are 5.6286 for 0 kGy, 1.8913 for 6 kGy, and 4.4538 for 18 kGy. In the third region, they are 1.8913 for 6 kGy and 4.4538 for 18 kGy. As can be observed, both linear areas have slopes (m) greater than 2, and the current follows the $I \sim e^{V^m}$ change. These findings demonstrate that space-charge restricted current, as opposed to ohmic and trap-charge limited currents, controls the dominant CCM in the reverse bias zone. When CCMs are valid, the slope value is closer to 1 and considerably higher than 2 with increasing irradiation.

The reverse bias IR versus VR characteristics are often distinct from the forward bias I_F versus V_F features. That is because the Poole-Frenkel and Schottky emissions (PFE and SE) theories can often explain the CCM in the reverse-bias zone. The I_R is described as follows when the PFE theory is prevalent[46,47]

$$I_R = I_0 \exp\left(\frac{\beta_{PF} V^{1/2}}{KTd^{1/2}}\right) \quad (9)$$

On the other side, the I_R is described by the following connection when the SE theory predominates.

$$I_R = AA^* T^2 \exp\left(\frac{-q\Phi_{B0}}{kT}\right) \exp\left(\frac{\beta_{sc} V^{1/2}}{KTd^{1/2}}\right) \quad (10)$$

In eq 10, the field-lowering coefficients of β_{PF} and β_{sc} are related to each other by $2\beta_{PF} = \beta_{sc}$. Figure 9b shows the variations of the $\ln(IR)$ versus $V_R^{1/2}$ for the Au/3% Gr-doped-PVA/n-type. It can be observed that the plots of these diodes have a good linear behavior both before and after β-irradiation.

4. CONCLUSIONS

The effects of β-irradiation on the semiconductors' electrical properties are very useful in a wide range of applications ranging from photodetectors to optical instruments. As explained in the present study, the structural properties of the device can be controlled using irradiation as a detector. However, ionizing radiation may pose several disadvantages such as interface traps, oxide trap charges, and defects in semiconductor devices. With the knowledge of similarities and differences between the structures and materials, we can better understand the radiation's effects. Moreover, the radiation affects the material's electrical parameters depending on the properties of the material. This is one of the most startling findings that we can learn by comparing the material's data.

In this study, the impacts of the β-irradiation on the Au/3% Gr-doped PVA/n-type Si structure's electrical parameters were investigated utilizing the $I-V$ data, which were measured across wide ranges of voltage (±4 V) and radiation dose (0, 6, and 18 kGy). To properly assess the impacts of β-irradiation on Au/3% Gr-doped PVA/n-Si structures, the key electrical parameters such as I_0, n, Φ_{B0}, R_s, RR, N_{ss}, and R_{sh} were acquired utilizing the $I-V$ characteristics of these structures before and after β-irradiation.

Additionally, the values of BH were computed as 0.888, 0.782, and 0.768 eV for 0, 6, and 18 kGy, respectively, while the values of n were computed as 3.21 for 0 kGy, 5.30 for 6 kGy, and 5.46 for 18 kGy. The R_{sh} values were computed as 0.755, 0.613, and 0.433 MΩ for 0, 6, and 18 kGy, respectively. The density of the structure increases owing to surface activation with β-irradiation compared with that of the structure that is not subjected to radiation. This was discovered by examining the structure's energy-dependent profiles of N_{ss} and considering the voltage dependency of n and Φ_{B0}. These experimental results explain that β-irradiation is more effective on the $I-V$ characteristics. Therefore, the fabricated Au/3%

https://doi.org/10.1021/acsomega.3c08449
ACS Omega 2024, 9, 23193−23201

Gr-doped- PVA/n-type SD can be utilized as a detector or radiation sensor.

Consequently, the following significant findings were obtained: (i) I_0 values increased with the rise in the irradiation doses. Deep levels acting as generating centers and the decrease in the BH were associated with this increase. (ii) The impacts of β-irradiation led to an increase in n values. The widening of the depletion layer and the decline in N_{ss} values under β-irradiation were attributed as the causes of this behavior. The third barrier was the Si dangling bond defect caused by radiation-induced faults. (iv) As β-irradiation doses rose, R_s and R_{sh} levels declined.

The Au/3% Gr-doped PVA/n-type Si structure may be employed as an MPS-type detector rather than an MIS/MOS type detector because of various advantages offered by the organic/polymer interlayer in terms of being affordable, flexible, and lightweight per molecule as well as needing little energy. This finding ensures the safe operation of satellite systems, biomedical equipment, and other electronic devices running under the β-irradiation impact. To conclude, the outcomes of this study will contribute to the growing body of knowledge in the field of nanomaterials and radiation-modulated properties, paving the way for innovative technological developments.

AUTHOR INFORMATION

Corresponding Author

Sema Bilge Ocak − *Graduate School of Natural and Applied Sciences, Department of Advanced Technologies, Gazi University, 06500 Ankara, Turkey;* orcid.org/0000-0002-0590-7555; Email: sbocak@gazi.edu.tr

Authors

Özlem Abay − *Graduate School of Natural and Applied Sciences, Department of Advanced Technologies, Gazi University, 06500 Ankara, Turkey; Turkish Energy, Nuclear and Mineral Research Agency, 06980 Ankara, Turkey*

Murat Ulusoy − *Faculty of Science, Department of Physics, Gazi University, 06500 Ankara, Turkey;* orcid.org/0000-0001-9842-0318

Esra Uyar − *Faculty of Science, Department of Physics, Gazi University, 06500 Ankara, Turkey*

Uğur Gökmen − *Faculty of Technology, Department of Metallurgical and Materials Engineering, Gazi University, 06500 Ankara, Turkey*

Complete contact information is available at: https://pubs.acs.org/10.1021/acsomega.3c08449

Notes

The authors declare no competing financial interest.

ACKNOWLEDGMENTS

The authors would like to express their sincere appreciation to the Scientific Research Projects Office of Gazi University for providing financial support for the study (project no. FGA-2023-8522 and FUİ-2023-8680).

REFERENCES

(1) Majewski, L. A.; Kingsley, J. W.; Balocco, C.; Song, A. M. Influence of processing conditions on the stability of poly(3-hexylthiophene)-based field-effect transistors. *Appl. Phys. Lett.* **2006**, *88*, 222108.

(2) Murphy, A. R.; Frechet, J. M. J. Organic semiconducting oligomers for use in thin film transistors. *Chem. Rev.* **2007**, *107* (4), 1066−1096.

(3) Keivanidis, P. E.; Greenham, N. C.; Sirringhaus, H.; Friend, R. H.; Blakesley, J. C.; Speller, R.; Campoy-Quiles, M.; Agostinelli, T.; Bradley, D. D. C.; Nelson, J. X-ray stability and response of polymeric photodiodes for imaging applications. *Appl. Phys. Lett.* **2008**, *92*, 023304.

(4) Kandemir, B. S.; Akay, D. "The effect of electron-phonon coupling in spin−orbit-coupled graphene.". *Phil. Mag.* **2017**, *97*, 2225−2235.

(5) Agostinelli, T.; Campoy-Quiles, M.; Blakesley, J. C.; Speller, R.; Bradley, D. D. C.; Nelson, J. A polymer/fullerene based photodetector with extremely low dark current for x-ray medical imaging applications. *Appl. Phys. Lett.* **2008**, *93* (20), 203305.

(6) Kandemir, B. S.; Akay, D. Photoinduced dynamical band gap in graphene: the effects of electron−phonon and spin−orbit interaction. *Phys. Status Solidi B* **2018**, *255* (10), 1800163.

(7) Knoll, G. *Radiation Detection and Measurement*. 3nd Ed. Wiley, 2000.

(8) Avouris, P.; Chen, Z.; Perebeinos, V. Carbon-based electronics. *Nat. Nanotechnol.* **2007**, *2* (10), 605−615.

(9) Ma, J.; Yeow, J. T. W.; Chow, J. C. L.; Barnett, R. B. A carbon nanotube-based radiation sensor. *Int. J. Rob. Autom.* **2007**, *22* (1), 49−58.

(10) Dürkop, T.; Getty, S. A.; Cobas, E.; Fuhrer, M. S. Extraordinary Mobility in Semiconducting Carbon Nanotubes. *Nano Lett.* **2004**, *4* (1), 35−39.

(11) Wei, B. Q.; Vajtai, R.; Ajayan, P. M. Reliability and current carrying capacity of carbon nanotubes. *Appl. Phys. Lett.* **2001**, *79* (8), 1172−1174.

(12) D'Andrade, B. W.; Forrest, S. R. White organic light-emitting devices for solid-state lighting. *Adv. Mater.* **2004**, *16* (18), 1585−1595.

(13) Gather, M. C.; Köhnen, A.; Falcou, A.; Becker, H.; Meerholz, K. Solution-Processed Full-Color Polymer Organic Light-Emitting Diode Displays Fabricated by Direct Photolithography. *Adv. Funct. Mater.* **2007**, *17* (2), 191−200.

(14) Aldissi, M. *Intrinsically Conducting Polymers: An Emerging Technology*; Kluwer Academic Publishers, 1993.

(15) Kavitha, C. M.; Eshwarappa, K. M.; Shilpa, M. P.; Shetty, S. J.; Surabhi, S.; Shashidhar, A. P.; Karunakara, N.; Gurumurthy, S. C.; Sanjeev, G. Tuning the optical and electrical properties by gamma irradiation of silver nanoparticles decorated graphene oxide on glutaraldehyde crosslinked polyvinyl alcohol matrix. *Mater. Res. Bull.* **2024**, *173*, 112685.

(16) Tamura, M.; Miyata, H.; Katsumata, M.; Matsuda, K.; Ueno, T.; Ito, D.; Suzuki, T. Beta particle detection efficiency of the radiation sensor made from a mixture of polyaniline and titanium oxide. *Nucl. Instr. Meth. Phys. Research A* **2016**, *828*, 176−180.

(17) Suzuki, T.; Miyata, H.; Katsumata, M.; Nakano, S.; Matsuda, K.; Tamura, M. Organic semiconductors as real-time radiation detectors. *Nucl. Instrum. Methods Phys. Research A* **2014**, *763*, 304−307.

(18) Dökme, İ.; Durmuş, P.; Altındal, Ş. Effects of gamma-ray irradiation on the C-V and G/ω-V characteristics of Al/SiO_2/p-Si (MIS) structures. *Nucl. Instrum. Methods Phys. Research B* **2008**, *266* (5), 791−796.

(19) Dökme, İ.; Altındal, Ş. The effect of gamma irradiation on electrical and dielectric properties of Al-TiW-Pd2Si/n-Si Schottky diode at room temperature. *Curr. Appl. Phys.* **2012**, *12* (3), 860−864.

(20) Altındal, Ş.; Tataroğlu, A.; Dökme, İ. Density of interface states, excess capacitance and series resistance in the metal−insulator−semiconductor (MIS) solar cells. *Sol. Energy Mater. Sol. Cells* **2005**, *85* (3), 345−358.

(21) Alptekin, S.; Altındal, Ş. A comparative study on current/capacitance:Voltage characteristics of Au/n-Si (MS) structures with and without PVP İnterlayer. *J. Mater. Sci.: Mater. Electron.* **2019**, *30*, 6491−6499.

(22) Sze, S. M.; Li, Y.; Ng, K. K. *Physics of Semiconductor Devices*; Wiley, 2021.
(23) Foxe, M.; Lopez, G.; Childres, I.; Jalilian, R.; Patil, A.; Roecker, C.; Boguski, J.; Jovanovic, I.; Chen, Y. P. Graphene field-effect transistors on undoped semiconductor substrates for radiation detection. *IEEE Trans. Nanotechnol.* **2012**, *11* (3), 581−587.
(24) Kotani, T.; Kawai, N.; Chiba, S.; Kitamoto, S. Development of a new radiation detector utilizing CNTs as anodes. *Physica E* **2005**, *29* (3−4), 505−509.
(25) Arora, N.; Sharma, N. N. Arc discharge synthesis of carbon nanotubes: Comprehensive review. *Diamond Relat. Mater.* **2014**, *50*, 135−150.
(26) Alialy, S.; Kaya, A.; Uslu, İ.; Altındal, Ş. Illumination and Voltage Dependence of Electrical Characteristics of Au/0.03 Graphene-Doped PVA/n-Si Structures via Capacitance/Conductance-Voltage Measurements. *Chin. Phys. Lett.* **2015**, *32* (11), 116102.
(27) Badila, M.; Godignon, Ph.; Millan, J.; Berberich, S.; Brezeanu, G. The electron irradiation effects on silicon gate dioxide used for power MOS devices. *Microelectron. Reliab.* **2001**, *41*, 1015−1018.
(28) Altındal, Ş.; Barkhordari, A.; Pirgholi-Givi, G.; Ulusoy, M.; Mashayekhi, H.; Özçelik, S.; Azizian-Kalandaragh, Y. Comparison of the electrical and impedance properties of Au/(ZnOMn:PVP)/n-Si (MPS) type Schottky-diodes (SDs) before and after gamma-irradiation. *Phys. Scr.* **2021**, *96* (12), 125881.
(29) Tamura, M.; Miyata, H.; Katsumata, M.; Matsuda, K.; Ueno, T.; Ito, D.; Suzuki, T. Beta particle detection efficiency of the radiation sensor made from a mixture of polyaniline and titanium oxide. *Nuclear Instruments and Methods in Physics Research A* **2016**, *828*, 176−180.
(30) Akay, D.; Ocak, S. B. Tuning the electrical properies with higher gamma-ray irradiation: Poly (methyl methacrylate)/lead oxide (PbO) composite nanostructures. *Surf. Rev. Lett.* **2020**, *27* (06), 1950156.
(31) Akay, D.; Gokmen, U.; Ocak, S. B. Ionizing Radiation Influence on Rubrene-Based Metal Polymer Semiconductors: Direct Information of Intrinsic Electrical Properties. *JOM.* **2020**, *72* (6), 2391−2397.
(32) Sharma, B. L. *Metal-Semiconductor Schottky Barrier Junctions and Their Applications*; Plenum Press: New York and London, 1984; .
(33) Werner, J. H.; Guttler, H. H. Barrier inhomogeneities at Schottky contacts. *J. Appl. Phys.* **1991**, *69* (3), 1522−1533.
(34) Ulusan, A. B.; Tataroğlu, A.; Altındal, Ş.; Azizian-Kalandaragh, Y. Photoresponse characteristics of Au/($CoFe_2O_4$-PVP)/n-Si/Au (MPS) diode. *Journal of Mater. Sci. Mater. Electron* **2021**, *32* (12), 15732−15739.
(35) Khalili, S.; Chenari, H. M.; Yıldırım, F.; Orhan, Z.; Aydoğan, S. Highly sensitive, self-powered photodetector based on reduced graphene oxide-polyvinyl pyrrolidone fibers (Fs)/p-Si heterojunction. *J. Alloys Compd.* **2021**, *889*, 161647.
(36) El-Mahalawy, A. M.; Salam, M. A. E. Fabrication and photoresponse characteristics of high rectification photodetector based on methyl violet nanoparticles-PVA/p-si heterojunction for optoelectronic applications. *Appl. Phys. A: Mater. Sci. Process.* **2020**, *126*, 393.
(37) Gündüz, B.; Turan, N.; Kaya, E.; Çolak, N. The photo-electrical properties of the p-Si/Fe(II)−polymeric complex/Au diode. *Synth. Met.* **2013**, *184*, 73−82.
(38) Ertuğrul, R.; Tataroğlu, A. Effects of gamma irradiation on electrical parameters of metal−insulator−semiconductor structure with silicon nitride interfacial insulator layer. *Radiat. Eff. Defects Solids* **2014**, *169* (9), 791−799.
(39) Norde, H. A modified forward I-V plot for Schottky diodes with high series resistance. *J. Appl. Phys.* **1979**, *50* (7), 5052−5053.
(40) Tataroğlu, A.; Altındal, Ş. Analysis of interface states and series resistance at MIS structure irradiated under ^{60}Co γ-rays. *Nucl. Inst. Methods in Physıcs Research.* **2007**, *580* (3), 1588−1593.
(41) Card, H. C.; Rhoderick, E. H. Studies of tunnel MOS diodes I. Interface effects in silicon Schottky diodes. *J. Phys. D: Appl. Phys.* **1971**, *4* (10), 1589−1601.
(42) Yerişkin, S. A.; Balbaşı, M.; Orak, İ. Frequency dependent electrical characteristics and origin of anomalous capacitance−voltage (C−V) peak in Au/(graphene-doped PVA)/n-Si capacitors. *J. Mater. Sci:Mater. Electron* **2017**, *28* (11), 7819−7826.
(43) Yerişkin, S. A.; Balbaşı, M.; Orak, İ. The effects of (graphene doped-PVA) interlayer on the determinative electrical parameters of the Au/n-Si (MS) structures at room temperature. *J. Mater. Sci.: Mater. Electron.* **2017**, *28* (18), 14040−14048.
(44) Rhoderick, E. H.; Williams, R. H. *Metal-Semiconductor Contacts*. 2 nd Ed, Clarendon Press, 1988.
(45) Kaya, A.; Vural, O.··.; Tecimer, H.; Demirezen, S.; Altındal, Ş. Frequency and voltage dependence of dielectric properties and electric modulus in Au/PVC+TCNQ/p-Si structure at room temperature. *Curr. Appl. Phys.* **2014**, *14* (3), 322−330.
(46) Buyukbas-Uluşan, A.; Yerişkin, S. A.; Tataroğlu, A.; Balbaşı, M.; Kalandaragh, Y. A. Electrical and impedance properties of MPS structure based on (Cu_2O-CuO-PVA) interfacial Layer. *J. Mater. Sci.: Mater. Electron.* **2018**, *29* (10), 8234−8243.
(47) Schroeder, H. Poole-Frenkel-effect as dominating current mechanism in thin oxide films-An illusion?! *J. Appl. Phys.* **2015**, *117* (21), 215103.

https://doi.org/10.1021/acsomega.3c08449
ACS Omega 2024, 9, 23193−23201